Inorganic Chemistry

Article

pubs.acs.org/IC

Topotactic Reduction Yielding Black Titanium Oxide Nanostructures as Metallic Electronic Conductors

Satoshi Tominaka*

International Center for Materials Nanoarchitectonics (WPI-MANA), National Institute for Materials Science (NIMS), Tsukuba, Ibaraki 305-0044, Japan

Supporting Information

ABSTRACT: Detailed analyses of reduced, single crystal, rutile-type TiO_2 via high-resolution transmission electron microscopy (TEM) are reported which reveal that the reduction proceeds topotactically via interstitial diffusion of Ti ions at low temperature, around 350 °C. This important finding encouraged the production of various nanostructured reduced titanium oxides from TiO_2 precursors with morphology retention, and in the process, the synthesis of black titanium oxide nanorods using TiO_2 nanorods was demonstrated. Interestingly, as opposed to the semiconductive behavior of Ti_2O_3 synthesized at high temperature, topotactically synthesized Ti_2O_3 exhibits metallic electrical resistance, and the value at room temperature is quite low (<6 μΩ m, comparable to graphite). These unique properties are probably due to the lattice strains generally observed for topotactically synthesized Ti_2O_3. This work shows that topotactically reduced titanium oxides can have fascinating properties as well as nanostructures.

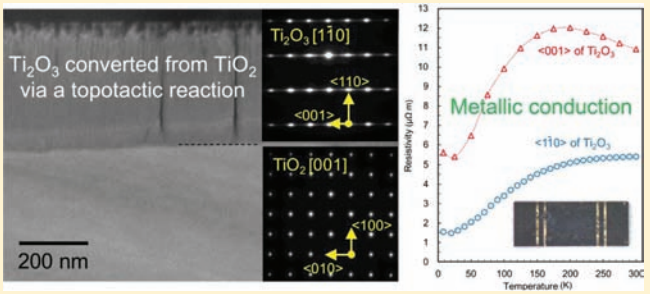

INTRODUCTION

Reduction treatment of titanium dioxide (TiO_2) has been widely conducted to yield electron-conductive and/or visible light-absorptive materials, which are important in a wide range of applications such as fuel cells[1] and photocatalysts.[2,3] In addition to properties related to their electronic structures, reduced titanium oxides are promising in terms of their abundance, chemical stability, and environmental friendliness. For example, an *n*-type semiconductor of nonstoichiometric TiO_{2-x} ($x < 0.1$) is widely prepared by reducing rutile-type TiO_2 (tetragonal, $P4_2/nmm$).[4,5] Further reduction yields a homologous series of stoichiometric titanium oxides of the form Ti_nO_{2n-1} ($4 \leq n \leq 10$), the so-called Magnéli phase, which consists of two-dimensionally ordered defect sites. Within the series, Ti_4O_7 (triclinic, $I\bar{1}$) has a metallic conductivity comparable to carbon materials at room temperature.[6] A stoichiometric phase of corundum-type Ti_2O_3 (hexagonal, $R\bar{3}c$) is a highly electrically conductive semiconductor (90 μΩ m, room temperature).[7] For the applications mentioned above, a synthetic route to access nanostructured reduced titanium oxides is required in order to increase the surface area, where catalytic reaction occurs and, also, to utilize their morphological merits; e.g., nanowires enhance electrical conduction because of a reduction in the interfaces between particles. However, the high temperature approaches generally used for reducing TiO_2 do not seem suitable due to particle growth even at temperatures (e.g., 465 °C)[8] far below the melting point of 1840 ± 10 °C.[4] In order to avoid such particle growth, two types of approaches have been reported: one is an encapsulation method using SiO_2,[9] and the other is a low-temperature approach using strongly reducing conditions.[3,10] Regarding the latter, Tominaka et al. used CaH_2, a strong reducing agent,[11] to reduce rutile-type TiO_2 nanoparticles at low temperature (350 °C), to yield corundum-type Ti_2O_3 nanoparticles of the same morphology as the parent TiO_2.[10]

Topotactic reactions, in which a component(s) of the parent crystal is exchanged with the surroundings while retaining one or several crystallographically equivalent orientations to the product,[12] are considered to be one of the most promising routes for the rational design of nanostructured materials by converting one phase into another with morphology retention.[13] If the low-temperature reduction of TiO_2 proceeds topotactically, it enables the design of nanostructured reduced titanium oxides by controlling the TiO_2 morphology using previously developed techniques.[14] Since the morphology of the parent is retained, the low-temperature reduction of rutile-type TiO_2 seems to be a topotactic reaction; however, since all of the oxygen ions in rutile are equivalent, the reaction mechanism does not appear to be deintercalation, which is typical of topotactic reactions, e.g., the deoxygenation of perovskites.[13,15,16] Thus, a detailed investigation of the mechanism of the low-temperature reduction of TiO_2 is of great importance to acquire a better understanding of these highly useful reduced titanium oxides.

Received: March 14, 2012
Published: June 6, 2012

dx.doi.org/10.1021/ic300557u | *Inorg. Chem.* 2012, 51, 10136−10140

Herein, the reduction of rutile TiO_2 is discussed from an atomic perspective in an effort to open a new route to rationally designed nanostructured reduced titanium oxide. First, the similarities and differences between the crystallographic orientations of the precursor TiO_2 and the reduced phase are investigated using TiO_2 single crystals (summarized in Figure 1a). Moreover, the potential difference in physical parameters from thermally equivalent phases is discussed on the basis of the magnitude of the electrical resistance as well as its unique temperature dependence. On the basis of the findings from the single crystal work, the transformation of rutile TiO_2 nanorods to Ti_2O_3 nanorods having the same morphology is demonstrated.

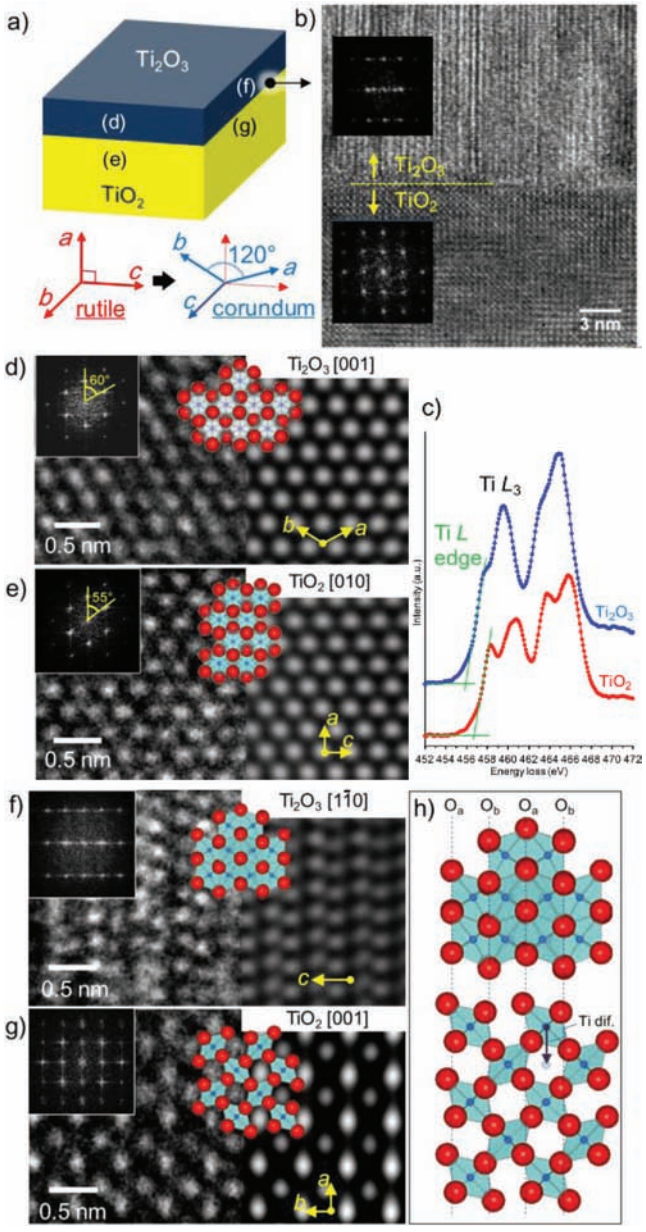

Figure 1. (a) Crystal orientation relationship between the parent (100)-oriented TiO_2 single crystal and the reduced phase formed near the surface, as determined by TEM observation. (b) High-resolution TEM image shows a clear boundary between the reduced phase and the TiO_2. (c) EELS of Ti edge. The cross-sectional atomic resolution TEM images of the reduced phase (d, f) and TiO_2 (e, g) reveal that the original *b*-axis of the TiO_2 corresponds to the *c*-axis of corundum Ti_2O_3 and the *a*-axis of the TiO_2 corresponds to the ⟨110⟩ direction of Ti_2O_3. The inset patterns are FFT images, and inverse FFT images are shown on the right side of the TEM images with superimposed structural diagrams (red: oxygen atoms; blue: titanium atoms). These data suggest the interstitial diffusion of Ti ions with the arrangement of O ions retained, as illustrated in (h).

EXPERIMENTAL SECTION

Synthesis. The mirror-polished, 0.5 mm thick single crystals were purchased from Fruuchi Chemical (Tokyo, Japan). After protecting the surface with a polymer film, the crystals were cut into 2 mm × 3 mm pieces using a DISCO DAD3220 dicing saw (Tokyo, Japan) and then cleaned by rinsing with acetone. Organic compounds were removed with oxygen plasma. The clean crystal was annealed in air at 1000 °C to decrease defects and then reduced with CaH_2 in an evacuated glass tube for 10 days at 350 °C. The CaO byproduct and residual CaH_2 were removed with 0.1 M NH_4Cl/CH_3OH and distilled water. The TiO_2 nanorods (no. FTL-100) were purchased from Ishihara Sangyo Kaisha (Osaka, Japan) and reduced with CaH_2 without further preparation.

Analyses. The cross-sectional transmission electron microscope (TEM) samples were prepared using the focused-ion beam and microsampling method on an FB-2100 FIB system (Hitachi High-Technologies, Tokyo, Japan). The TEM observation and electron energy loss spectroscopy (EELS) measurements were performed using a JEM-2100F microscope (JEOL, Tokyo Japan) at 200 kV. The Ti $L_{3,2}$ edge spectra were corrected with background subtraction based on a power law and then with energy-scale calibration using the O *K* edge peak position of the unreacted TiO_2 region (531.0 eV).[17]

SEM observations were performed using an SU-8000 microscope (Hitachi High-Technologies, Tokyo, Japan) at 1 kV (retarding mode) without surface coating. The powder X-ray diffraction (XRD) patterns were collected using an X'Pert diffractometer (PANalytical, Tokyo, Japan) equipped with a graphite monochromator and Cu Kα radiation (λ = 1.5418 Å). The diffuse reflectance spectra were obtained using a V-570 UV−vis−NIR spectrometer (JASCO, Tokyo, Japan) with an ISN-470 integrating sphere detector in the wavelength range of 2000 to 220 nm. The powder samples for this measurement were diluted with dry KCl powder to be 1 wt %. The raw diffuse reflectance spectra were converted into the Kubelka−Munk (K-M) function.

The temperature dependence of the resistance was measured from 8 to 300 K at ca. 1.2×10^{-5} Pa using a four probe method (bias: ± 0.5 V) with a GRAIL 10-408040LV cryogenic electrical characteristic measurement system (Nagase Techno-Engineering, Tokyo, Japan) and a 4200-SCS semiconductor characterization system (Keithley Instruments, Tokyo, Japan). The reduced single crystals of (100)-oriented rutile TiO_2 were carefully cut into 2 mm × 5 mm pieces using the dicing saw. Then, four Au lines 100 μm wide (100 nm thick with a 10 nm Ti adhesion layer) were deposited by electron beam evaporation through a Si stencil mask. The width and length of the conduction pathway was defined by the mask. The thickness of the reduced region was measured by cross-sectional TEM observation of the fabricated samples using a focused ion beam. The reacted region was around 400 nm thick.

RESULTS AND DISCUSSION

In the cross-sectional TEM images of the sample prepared from a $(100)_R$-oriented TiO_2 plate, a clear interface was observed between the reduced region (ca. 200 nm thick) and the unreacted TiO_2 region (Figure 1b). (An "R" subscript is used for rutile, and "C" is used for corundum.) In the EELS (Figure 1c), the Ti edge of Ti_2O_3 was observed at 456.2 eV, which is lower than that of TiO_2 at 456.8 eV, indicating the reduction of Ti^{4+} to Ti^{3+}. The peak splitting of the L_3 edge is accounted for by the Jahn−Teller effect on the Ti 3*d* orbital; i.e., there exists tetragonal distortion for the TiO_6 octahedra of TiO_2, and trigonal distortion for Ti_2O_3 (Figure S1, Supporting Informa-

dx.doi.org/10.1021/ic300557u | *Inorg. Chem.* 2012, 51, 10136−10140

tion).[17] The peak of the left Ti L_3 edge at 457.7 eV is less intense than the right peak at 459.5 eV for the reduced layer, also reflecting the formation of Ti^{3+} ions. Thus, the reduction treatment successfully formed a single crystal-like Ti_2O_3 layer on the TiO_2 crystal, which was further confirmed by electron diffraction and the following TEM analyses.

Crystallographic orientation details were determined from the atomic resolution TEM images (Figures 1d−g). Clear crystal orientation relationships of $[010]_R \parallel [001]_C$, $[001]_R \parallel [1\bar{1}0]_C$, and $[100]_R \parallel [110]_C$ were found, and thus, this low-temperature reduction of rutile TiO_2 is a topotactic reaction. In view of the oxygen atom arrangements, rutile TiO_2 contains nearly close-packed oxygen planes perpendicular to the $[100]_R$ and $[010]_R$ directions (Figure 1h), but only the planes perpendicular to $[010]_R$ transformed into the hexagonal close-packed planes of Ti_2O_3. Since the motion of oxygen defects in rutile is vacancy diffusion,[18] frameworks consisting of similar oxygen arrangements are considered to retain the single crystal-like domain.

Since the different crystal orientations in Ti_2O_3 were derived from the crystallographically equivalent directions of rutile ($[100]_R$ and $[010]_R$), a further understanding of the conversion mechanism is necessary. Only the $[010]_R$ direction converted into the $[001]_C$ direction, along which the face-sharing octahedra of Ti_2O_3 were aligned. These face-sharing octahedral sites were formed by the interstitial diffusion of Ti^{3+} ions generated from the charge compensation for oxygen vacancies.[18] The formation of oxygen vacancies should be immediately accompanied by interstitial Ti^{3+} diffusion to adjacent octahedral vacancy sites, because the Ti diffusion is estimated to be ca. 45 times faster than the oxygen vacancy diffusion at the reaction temperature of 350 °C (details are available in the Supporting Information).[18] This is consistent with experimental fact; that is, the absence of an intermediate layer between TiO_2 and Ti_2O_3 (Figure 1b). Thus, among the four equivalent $\langle 100\rangle_R$ directions of Ti diffusion, the direction toward the unreacted region, or opposite to the deoxygenation direction, is reasonably considered to be dominant.

In order to verify this hypothesis of the effect of geometrical anisotropy, the reduction of rutile single crystals of a different orientation was also analyzed. The reduced $(110)_R$-oriented TiO_2 (Supporting Information, Figure S3) contains (i) large Ti_4O_7 domains of two different crystallographic orientations near the TiO_2 parent, (ii) small Ti_2O_3 domains near the surface, and (iii) less ordered crystalline phases assignable to tiny crystallites of Ti_4O_7 between those regions. These results clearly indicate that face-sharing TiO_6 octahedra were formed along two different directions, $[100]_R$ and $[010]_R$, which are geometrically equivalent in $(110)_R$-oriented TiO_2. The reduced region was thicker (ca. 1.8 μm) than in $(100)_R$-oriented TiO_2, suggesting faster diffusion of oxygen vacancies in Ti_4O_7 or in a less ordered region than in the close-packed oxygen of the Ti_2O_3 phase. The reduced $(001)_R$-oriented TiO_2 (Figure S4, Supporting Information) was black, as were the previous two single crystals, but neither Ti_2O_3 nor Ti_4O_7 was observed. In this single crystal, all four crystallographically equivalent directions $\langle 100\rangle_R$, along which both macroscopic Ti diffusion and oxygen vacancy diffusion are preferred,[19,20] are perpendicular to the oxygen vacancy diffusion. This fact strongly supports the thought that interstitial diffusion of Ti ions in the direction opposite to the oxygen vacancies is important.

Therefore, the topotactic reaction of TiO_2 to Ti_2O_3 is found to be dominated by both the crystallographic orientation and the geometry of the crystals. These two factors determine the diffusion rate of oxygen vacancies and the nucleation rate of the Ti_2O_3 phase. In $(100)_R$-oriented TiO_2, the latter was considered sufficiently faster than the former because of the exactly opposite diffusion directions of the Ti ions ($[\bar{1}00]_R$) and the oxygen vacancies ($[100]_R$), thus a single crystal-like Ti_2O_3 layer was uniformly formed. In $(110)_R$-oriented TiO_2, the nucleation was considered to be slow because of the presence of two different diffusion directions of the Ti ions ($[\bar{1}00]_R$ and $[0\bar{1}0]_R$), and Ti_2O_3 phases of two different crystallographic orientations were formed.

In view of the crystal habits of tetragonal TiO_2 and hexagonal Ti_2O_3, this topotactic route is of practical importance because the transformation from TiO_2 is expected to produce Ti_2O_3 retaining the crystal habit of TiO_2. Thus, the transformation of single-crystalline TiO_2 rectangular nanorods 50−200 nm wide into single-crystalline Ti_2O_3 nanorods was explored. The XRD data of the reduced rod was confirmed to be of a corundum structure assignable to the Ti_2O_3 phase (Figure 2a). The XRD pattern contains several additional faint peaks attributable to Ti_4O_7 and TiO_2. The morphology of the TiO_2 nanorods was retained (Figure 2b,c) except for a slightly roughened surface of Ti_2O_3. Moreover, the crystal domain was also retained as judged from the single crystalline domain revealed by selected area electron diffraction patterns (Figure 2d). The powder was bluish black (Figure 2e, inset pictures) and exhibited a huge light absorption peak at 815 nm, as well as a small one around 400 nm (Figure 2e), which are typical of Ti_2O_3.[21] These data confirm that the topotactic reduction reaction of rutile TiO_2 successfully yields corundum Ti_2O_3.

Finally, in order to demonstrate the potential of such topotactically reduced titanium oxides, their electronic resistance was investigated. The temperature dependence of the electrical resistance of the reduced $(100)_R$ TiO_2 was measured using a four probe method from 8 to 300 K, and then, the resistance values were transferred into resistivity on the basis of the dimensions acquired from microscope images and cross-sectional high-angle annular dark-field scanning transmission electron microscope (HAADF-STEM) images (Figure 3). In general, as an electrical conductor, the pure Ti_2O_3 phase is known to be a highly conductive semiconductor (90 $\mu\Omega$ m) associated with a narrow bandgap below 400 K, which becomes a metallic conductor (3 $\mu\Omega$ m) above 500 K.[22] In contrast to pure Ti_2O_3 synthesized at high temperature, the resistance behavior of Ti_2O_3 synthesized at low temperature was metallic, even below 100 K, as found from a gradual resistance increase with temperature in that temperature range. Around room temperature, the behavior became semimetallic, although the resistance value was still quite low (<6 $\mu\Omega$ m for $\langle 1\bar{1}0\rangle_C$), a value comparable to graphite. The resistivity value was a few times larger along the $\langle 001\rangle_C$ direction than along the $\langle 1\bar{1}0\rangle_C$ direction. This is probably attributable to cracks anisotropically formed along the $\langle 1\bar{1}0\rangle_C$ direction and/or to low crystallinity along the $\langle 001\rangle_C$ direction, as suggested by the streaks observed along this direction in the ED pattern (Figure 3c).

The fascinatingly low resistance can be elucidated in terms of the frontier molecular orbital of a corundum Ti_2O_3 and the lattice strains of the topotactically synthesized Ti_2O_3. In corundum Ti_2O_3, the Ti^{3+} ions of the TiO_6 octahedra form face-sharing pairs along the *c* axis, each of which shares edges with a different pair in the *ab* plane. The 3*d* electrons are allocated in nondegenerate molecular orbitals formed between

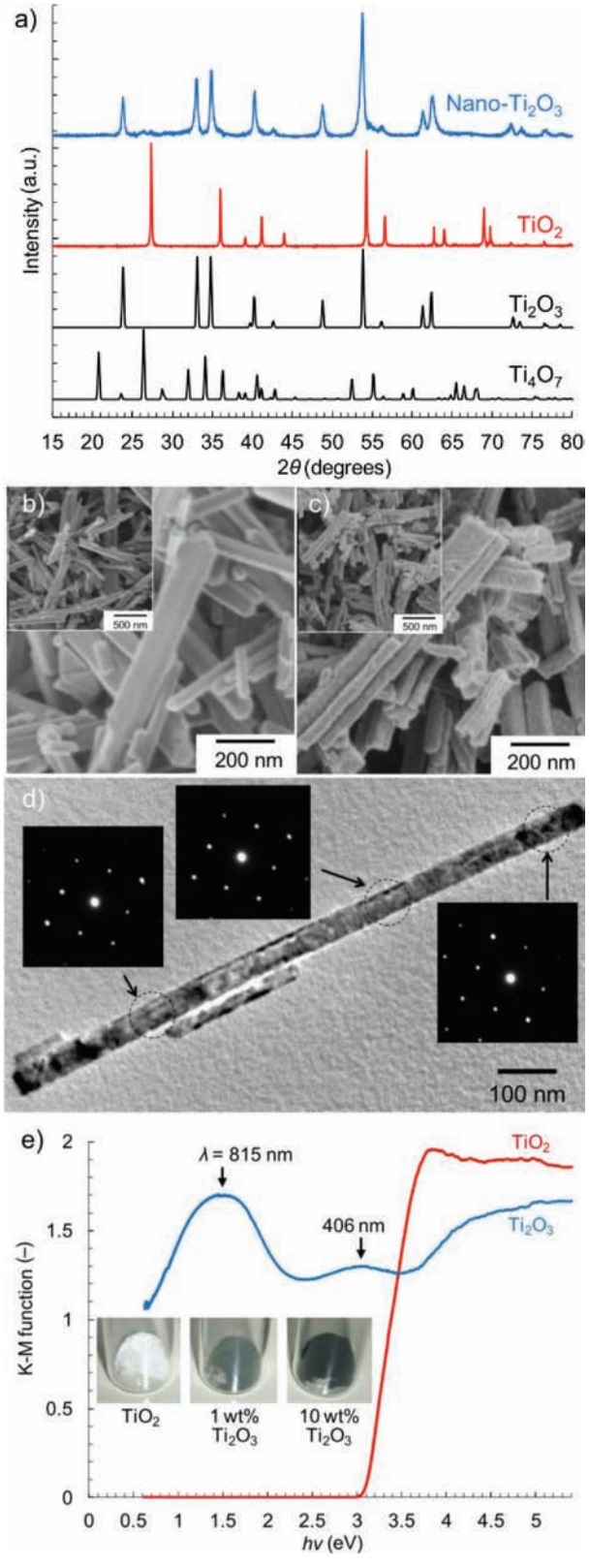

Figure 2. Characterization of the reduced titanium oxide nanorods. (a) Powder XRD patterns collected from Ti_2O_3 nanorods (blue) and the precursor TiO_2 (red) are compared with calculated patterns (black) for bulk Ti_2O_3 (ICSD 9646) and Ti_4O_7 (ICSD 48131). SEM images of TiO_2 (b) and Ti_2O_3 (c) at a low acceleration voltage of 1.0 keV. (d) TEM image and ED patterns confirm retention of the crystal domain. (e) Light absorption spectra of the reduced sample (blue) and the parent (red).

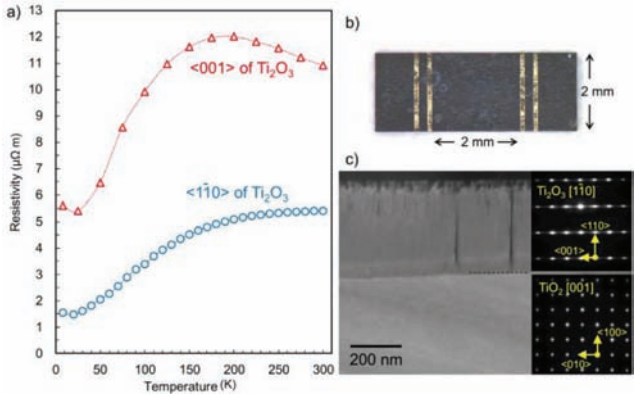

Figure 3. (a) Temperature dependence of electronic resistance measured along two different crystallographic directions in Ti_2O_3 prepared by reducing single crystals of (100)-oriented rutile TiO_2. (b) Plan-view photograph of a sample with Au current collectors. (c) Cross-sectional HAADF-STEM image for measurement of the thickness of the Ti_2O_3 phase, which can be confirmed by selected area electron diffraction patterns from the parent TiO_2. The boundary between Ti_2O_3 and TiO_2 was observed (dotted line).

face-sharing sites, the highest occupied molecular orbital (HOMO), and these localized electron pairs can transfer through 2-fold degenerate molecular orbitals formed between Ti ions of edge-sharing sites, the lowest unoccupied molecular orbital (LUMO). The gradual semiconductor-to-metal transition of Ti_2O_3, which commences around 160 °C, is accompanied with a slight expansion of the Ti−Ti distance of face-sharing pairs (a = 5.1570 Å, c = 13.610 Å at 23 °C; a = 5.1251 Å, c = 13.957 Å at 595 °C).[23] The lattice expansion along the c axis is believed to shift the HOMO upward to overlap with the LUMO, in accordance with the conventional Goodenough model.[23,24] In this view, for topotactically synthesized Ti_2O_3, with a lattice slightly expanded along the c axis and highly contracted in the ab plane (a = 5.0475 Å, c = 13.7516 Å at room temperature; data for the nanoparticles),[10] the downward shift of the LUMO associated with the contraction of the ab plane is considered to be the primary origin of the metallic state. Further details of the origin of the lattice strain and the unique electronic states are under investigation.

■ CONCLUSION

The transformation of rutile-type TiO_2 to corundum-type Ti_2O_3 during low-temperature reduction is concluded to be a topotactic reaction. This reaction successfully retained the crystal habit of the rutile parent as demonstrated by the conversion of TiO_2 nanorods into Ti_2O_3 nanorods. As opposed to Ti_2O_3 synthesized via a conventional route, topotactically synthesized Ti_2O_3 exhibits (semi)metallic electronic conduction. This fact indicates that the method is promising to access narrow- or zero-gap titanium-based oxide materials having nanostructures, which can be used in a variety of applications. Since such nanostructured reduced titanium oxides are novel, further investigations into their physical properties and electronic states are of great importance and will be reported in the near future.

dx.doi.org/10.1021/ic300557u | *Inorg. Chem.* 2012, 51, 10136−10140

■ ASSOCIATED CONTENT

Supporting Information

Additional data on the reduced $(100)_{R}$-, $(110)_{R}$-, and $(001)_{R}$-oriented TiO_2. Calculation of diffusion constant. This material is available free of charge via the Internet at http://pubs.acs.org.

■ AUTHOR INFORMATION

Corresponding Author

*Address: International Center for Materials Nanoarchitectonics (WPI-MANA), National Institute for Materials Science (NIMS), Namiki 1-1, Tsukuba, Ibaraki 305-0044, Japan. E-mail: TOMINAKA.Satoshi@nims.go.jp. Phone: +81-29-860-4594.

Notes

The authors declare no competing financial interest.

■ ACKNOWLEDGMENTS

This work was supported by a World Premier International Research Center Initiative (WPI-MANA), MEXT, Japan. The authors thank Y. Tsujimoto (NIMS) for help in the reduction treatment and XRD experiments, Y. Matsushita (NIMS) for discussion and comments, K. Kimoto (NIMS) for TEM data discussion, Y. Nemoto (NIMS) for help in the TEM observation, and T. Narushima (NIMS) for help in the TEM sample preparation.

■ REFERENCES

(1) Ioroi, T.; Senoh, H.; Yamazaki, S. I.; Siroma, Z.; Fujiwara, N.; Yasuda, K. *J. Electrochem. Soc.* **2008**, *155*, B321−B326.
(2) Gratzel, M. *Nature* **2001**, *414*, 338−344.
(3) Chen, X.; Liu, L.; Yu, P. Y.; Mao, S. S. *Science* **2011**, *331*, 746−750.
(4) Grant, F. A. *Rev. Modern Phys.* **1959**, *31*, 646−674.
(5) Tropov, N. A.; Barzakovsky, B. P.; Bndri, I. A.; Udalov, Y. P. *Phase Diagrams of Metal Oxides (originally in Russ. and translated into Jpn.)*; Soviet Academy of Science: Leningrad, USSR, 1970.
(6) Acha, C.; Monteverde, M.; Nunez-Regueiro, M.; Kuhn, A.; Franco, M. A. A. *Eur. Phys. J. B* **2003**, *34*, 421−428.
(7) Honig, J. M.; Reed, T. B. *Phys. Rev.* **1968**, *174*, 1020−1026.
(8) Gribb, A. A.; Banfield, J. F. *Am. Mineral.* **1997**, *82*, 717−728.
(9) Ohkoshi, S.; Tsunobuchi, Y.; Matsuda, T.; Hashimoto, K.; Namai, A.; Hakoe, F.; Tokoro, H. *Nat. Chem.* **2010**, *2*, 539−545.
(10) Tominaka, S.; Tsujimoto, Y.; Matsushita, Y.; Yamaura, K. *Angew. Chem., Int. Ed.* **2011**, *50*, 7418−7421.
(11) Hayward, M. A.; Cussen, E. J.; Claridge, J. B.; Bieringer, M.; Rosseinsky, M. J.; Kiely, C. J.; Blundell, S. J.; Marshall, I. M.; Pratt, F. L. *Science* **2002**, *295*, 1882−1884.
(12) Gunter, J. R.; Oswald, H. R. *Bull. Inst. Chem. Res., Kyoto Univ.* **1975**, *53*, 249−255.
(13) Ranmohotti, K. G. S.; Josepha, E.; Choi, J.; Zhang, J. X.; Wiley, J. B. *Adv. Mater.* **2011**, *23*, 442−460.
(14) Yang, H. G.; Sun, C. H.; Qiao, S. Z.; Zou, J.; Liu, G.; Smith, S. C.; Cheng, H. M.; Lu, G. Q. *Nature* **2008**, *453*, 638−U634.
(15) Tsujimoto, Y.; Tassel, C.; Hayashi, N.; Watanabe, T.; Kageyama, H.; Yoshimura, K.; Takano, M.; Ceretti, M.; Ritter, C.; Paulus, W. *Nature* **2007**, *450*, 1062−1065.
(16) Hayward, M. A.; Green, M. A.; Rosseinsky, M. J.; Sloan, J. *J. Am. Chem. Soc.* **1999**, *121*, 8843−8854.
(17) Stoyanov, E.; Langenhorst, F.; Steinle-Neumann, G. *Am. Mineral.* **2007**, *92*, 577−586.
(18) Fisher, D. J., Ed. *Defect and diffusion forum*; Scitec Publications: Uetikon, Zurich, Switzerland, 1999; pp 252−253.
(19) Iguchi, E.; Yajima, K. *J. Phys. Soc. Jpn.* **1972**, *32*, 1415−1421.
(20) Steele, J. L.; Mccartne, E. *Nature* **1969**, *222*, 79.
(21) Lu, S. S. M.; Pollak, F. H.; Raccah, P. M. *Phys. Rev. B* **1978**, *17*, 1970−1975.
(22) Honig, J. M.; Reed, T. B. *Phys. Rev.* **1968**, *174*, 1020−1026.
(23) Rice, C. E.; Robinson, W. R. *Mater. Res. Bull.* **1976**, *11*, 1355−1359.
(24) Shin, S. H.; Aggarwal, R. L.; Lax, B.; Honig, J. M. *Phys. Rev. B* **1974**, *9*, 583−590.